Atmos. Meas. Tech., 5, 2635–2646, 2012
www.atmos-meas-tech.net/5/2635/2012/
doi:10.5194/amt-5-2635-2012

Atmospheric Measurement Techniques

Corrections for OMI SO_2 BRD retrievals influenced by row anomalies

H. Yan[1,2], L. Chen[1], J. Tao[1], L. Su[1], J. Huang[3], D. Han[4], and C. Yu[1,2]

[1]State Key Laboratory of Remote Sensing Science, Jointly Sponsored by the Institute of Remote Sensing Applications of Chinese Academy of Sciences and Beijing Normal University, Beijing, China
[2]Graduate University of the Chinese Academy of Sciences, Beijing, China
[3]Key Laboratory of Digital Earth Science, Center for Earth Observation and Digital Earth Chinese Academy of Sciences, Beijing, China
[4]Normal College, Qingdao University, Qingdao, China

Correspondence to: L. Chen (lfchen@irsa.ac.cn)

Received: 9 January 2012 – Published in Atmos. Meas. Tech. Discuss.: 27 January 2012
Revised: 3 September 2012 – Accepted: 8 October 2012 – Published: 6 November 2012

Abstract. Since June 2007, the Ozone Monitoring Instrument (OMI) Earth radiance data at specific viewing angles have been affected by the row anomaly, which causes large biases in sulfur dioxide (SO_2) columns retrieved using the band residual difference (BRD) algorithm. To improve global measurements of atmospheric SO_2 from OMI, we developed two correction approaches for the row anomaly effects in the northern latitudes and along the full orbit. Firstly the residual correction approach with median residual from a sliding 10° latitude range, and with that near the Equator was used to remove the anomalous high SO_2 columns in the northern latitudes. Secondly, in the case of the row anomaly along the full orbit, the SO_2 biases caused by the anomalous ozone (O_3) column and underestimated Lambertian effective reflectivity (LER) were reduced, respectively, by using unaffected adjacent O_3 column and residual correction with median residual from a sliding 10° latitude range. Comparisons with the OMI SO_2 columns processed with median residual from a sliding 30° latitude range have illustrated the drastic improvements of our correction approaches under row anomaly conditions. The consistencies among the SO_2 columns inside and outside the row anomaly areas have also demonstrated the effectiveness of our correction approaches under row anomaly conditions. The analyses of the underestimation and the errors caused by the O_3 column and LER were conducted to understand the limitations of our correction approaches. The proposed approaches for the row anomaly effects can extend the valid range of OMI SO_2 Planetary Boundary Layer (PBL) data produced using the BRD algorithm.

1 Introduction

Sulfur dioxide (SO_2) is a short-lived gas, released primarily by anthropogenic activities (e.g., smelting of sulfur ore, combustion of coal, emissions from motor vehicles) and natural phenomena (e.g., volcanic and sulfur minerals decomposition) (Cullis and Hirschler, 1980; Seinfeld and Pandis, 1998; Finlayson-Pitts and Pitts, 2000). There is concern about the impact of SO_2 on the radiation balance of the atmosphere through the formation of sulfate aerosols, as well as on ecosystems and human health (Intergovernmental Panelon Climate Change (IPCC), 2001).

Since the Nimbus-7 Total Ozone Mapping Spectrometer's (TOMS) first sighting of SO_2 cloud from El Chichón's eruption in 1982 (Krueger, 1983), satellite remote sensing technology has been playing an important role in the field of atmospheric monitoring. Later, Global Ozone Monitoring Experiment (GOME), SCanning Imaging Absorption spectroMeter for Atmospheric CartograpHY (SCIAMACHY), and Ozone Monitoring Instrument (OMI) were developed, and all these instruments have high SO_2 monitoring capability. OMI, which was launched on the EOS/Aura platform in July 2004, combines the hyperspectral measurements of GOME and SCIAMACHY with improved nadir spatial resolution ($13\times24\,km^2$), and achieves the daily global monitoring of short-lifetime SO_2. It measures solar radiation backscattered by the Earth's atmosphere in the sun-synchronous polar orbit with 13:45 local Equator crossing time, and makes simultaneous measurements in a swath of

about 2600 km, divided into 60 pixels (Levelt et al., 2006). OMI's high sensitivity to SO_2 and low noise enables detection of low near-surface SO_2 emission, long-range tracking of SO_2 cloud in the upper troposphere and lower stratosphere (Krueger et al., 2002; Krotkov et al., 2008; Carn et al., 2007; Li et al., 2010; Yan et al., 2012).

Approaches for retrieval of SO_2 from satellite instruments have been developed and applied to detection of volcanic SO_2 for aviation (Yang et al., 2007; Krotkov et al., 2006; Rix et al., 2010; Lee et al., 2008; Corradini et al., 2009; Realmuto et al., 1994). Among the ultraviolet (UV) inversion algorithms of SO_2, differential optical absorption spectroscopy (DOAS) (Platt, 1994; Platt and Stutz, 2008), linear fit algorithm (LF) (Yang et al., 2007) and band residual difference algorithm (BRD) (Krotkov et al., 2006) are sensitive to high volcanic SO_2 in the upper troposphere or the low stratosphere (Yang et al., 2007; Rix et al., 2010; Lee et al., 2008). For OMI measurements, operational SO_2 Planetary Boundary Layer (PBL) data have been processed with the BRD algorithm (Krotkov et al., 2006), which takes advantage of the largest differential SO_2 cross sections in the OMI UV2 spectral region (310–380 nm). OMI-retrieved SO_2 PBL columns have been used to study regional emissions, synoptic pollution events and large point emission sources (Krotkov et al., 2008; Carn et al., 2007; Li et al., 2010; Yan et al., 2012).

Background correction is necessary for atmospheric SO_2 column retrieval, because retrieval errors and measurement noises can result in false SO_2 columns over regions with very low SO_2 emission. The DOAS retrieval algorithm uses a reference sector approach by subtracting the presumably SO_2 free reference data (generally in the Pacific Ocean area) to correct the latitudinal varying background errors (Khokhar et al., 2005; Richter et al., 2006). However, the forward model errors and satellite measurement errors that affect the SO_2 retrieval are dynamic over the globe and vary with season, latitude, observation geometry, O_3 column amount, surface reflectivity, etc. Therefore, using a fixed reference sector for the empirical correction of SO_2 retrieval would possibly bring new error sources.

Yang developed a sliding median approach for residual correction, which has been applied to OMI SO_2 products (Krotkov et al., 2008; Yang et al., 2007). This approach calculates the median residual for each cross-track pixel from a sliding group of pixels covering about 30° latitude along the orbit track, and then subtracts the sliding median value for each spectral band and each cross-track position to reduce the error interference for the centered pixels. However, this approach with median residual from a sliding 30° latitude range has been unsuitable for the cases with row anomaly since June 2007, and results in large biases in the retrieved SO_2 columns.

To improve the retrieval of SO_2 when row anomaly occurs, we developed two correction approaches for the row anomaly effects in the northern latitudes and along the full orbit. Firstly, the residual correction approach with median residual from a sliding 10° latitude range and with those near the Equator was used to remove the anomalous high SO_2 columns in the northern latitudes (see Sect. 4.1). Different from those in the northern latitudes, the SO_2 column biases along the full orbit are mainly caused by the anomalous O_3 columns and underestimated Lambertian effective reflectivity (LER), which are used as inputs in the BRD algorithm (see Sect. 4.2). Our second correction approach involved reducing the SO_2 biases along the full orbit by using unaffected adjacent O_3 column and residual correction with median residual from a sliding 10° latitude range. The OMI SO_2 columns from November 2008 to November 2009 were processed with proposed approaches in this paper, and the results were compared with that processed with median residual from a sliding 30° latitude range suggested by Yang (Yang et al., 2007). Comparison results illustrate the drastic improvements invoked by these correction approaches under row anomaly conditions.

The paper is organized as follows. In Sect. 2, an overview of BRD algorithm and parameters needed for the forward computation are presented. In Sect. 3, detailed analysis of OMI data error sources is conducted to understand the characteristics of measurement error sources and the row anomaly effects. Correction approaches for improvement of SO_2 retrievals with row anomaly are described in detail in Sect. 4. In Sect. 5, to evaluate the effectiveness of our correction approaches, several orbits covering days with row anomaly effects from November 2008 to November 2009 are selected to compare the SO_2 columns before and after processed with proposed correction approaches. The limitations of our correction approaches are also discussed in Sect. 5. Section 6 summarizes the findings.

2 OMI SO_2 PBL columns retrieval

2.1 BRD algorithm overview

SO_2 PBL columns are retrieved from OMI measurements of the solar irradiance and the Earth radiance (Van den Oord et al., 2002) in the ultraviolet (310.8 nm to 314.4 nm) using the BRD algorithm (Krotkov et al., 2006). In the BRD algorithm, the TOMS total ozone retrieval (OMTO3) (Bhartia and Wellemeyer, 2002) is firstly used to derive an initial estimate of total ozone (assuming zero SO_2), as well as the wavelength-independent LER. The OMTO3 algorithm accomplishes this by matching calculated radiances using TOMS forward model (TOMRAD) (Dave, 1964) to the measured radiances at a pair of wavelengths (317.5 nm and 331.2 nm under most conditions). The measurements at 317.5 nm are used to derive total ozone; the measurements at 331.2 nm provide LER. Then the retrieved O_3 column and LER are used as inputs in TOMRAD to obtain the calculated N-pair values ($N\text{-pair} = N(\lambda_{\text{short}}) - N(\lambda_{\text{long}})$, $N = -100 \cdot \log_{10}(I/F)$, I is Earth radiance and F is solar irradiance)

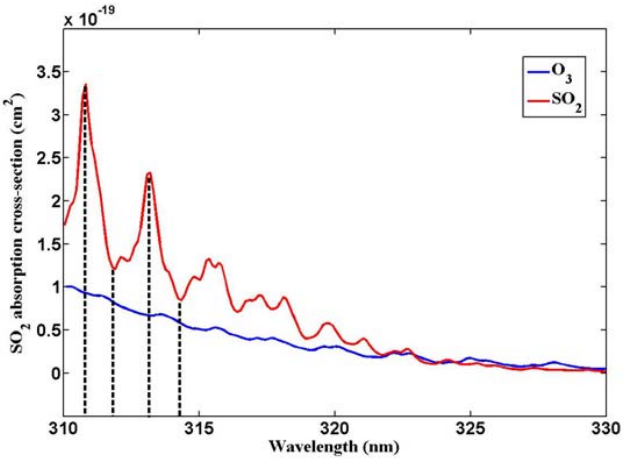

Fig. 1. O_3 and SO_2 absorption spectrum in UV band. The black dashed lines label the four wavelengths (310.8, 311.9, 313.2, and 314.4 nm) used in the SO_2 BRD retrieval.

at the three wavelength pairs (P1: 310.8 vs. 311.9 nm; P2: 311.9 vs. 313.2 nm; P3: 313.2 vs. 314.4 nm) (Fig. 1). The residuals at these three wavelength pairs are calculated as the differences between the measured and calculated N-pair values (N-pair $= N(\lambda_{\text{short}}) - N(\lambda_{\text{long}})$). In the presence of SO_2, the residuals at three wavelength pairs are positively correlated with atmospheric SO_2 columns and three SO_2 columns in the same OMI pixel can be obtained. The final SO_2 column is the average of three SO_2 columns.

The BRD algorithm takes advantage of the bands centered at the local minima and maxima of the SO_2 absorption cross section between 310.8 and 314.4 nm (Bogumil et al., 2003) (Fig. 1), thereby maximizing the detection sensitivity to low SO_2 columns. Note that the negative SO_2 columns in this paper are caused by the interference between the SO_2 and O_3 absorption and can typically indicate very low SO_2 columns.

2.2 Forward model

TOMRAD accounts for all orders of scattering and gaseous absorptions (Dave, 1964) and was adopted to derive the calculated N-pair value in this paper. In the forward computation, the calculated N-pair value is determined as follows: (1) OMI level 2 O_3 column and LER retrieved by OMTO3 algorithm as inputs; (2) ozone profiles determined by matching the OMTO3 O_3 column to the TOMS-V8 ozone profile climatology, which varies with latitude and ozone column (Bhartia and Wellemeyer, 2002; Wellemeyer et al., 1997; McPeters et al., 2007); (3) linear interpolation with eight solar zenith angles (15°, 30°, 45°, 60°, 70°, 77°, 84°, and 88°) and five viewing zenith angles (15°, 30°, 45°, 60°, and 70°); (4) the opaque surfaces characterized by the LER obtained from OMTO3 algorithm; (5) the initial guess of the zero SO_2 column and the surface pressure of 1013.25 hPa; and finally (6) the calculated N-pair value as a function of O_3 column, LER, solar zenith angle (SZA), view zenith angle (VZA) and azimuth angle (AZ) is estimated at the three wavelength pairs.

3 Data error sources

3.1 Systematic measurement errors

OMI makes the measurements of the Earth radiance and the solar irradiance in a Sun-synchronous orbit and provides fully contiguous coverage of the globe with 14 or 15 orbits daily. The measurements of solar irradiance are performed once a day. One solar irradiance product is nominally used for the operational processing of the Earth radiance measurements of one day ($\sim$ 14 orbits).

OMI level 1b solar irradiances and Earth radiances are pre-calibrated using the Ground Data Processing Software (GDPS) developed by Dutch Space in the Netherlands (van den Oord et al., 2006). However, even after GDPS calibration, the remaining systematic measurement errors (i.e., solar irradiance errors and Earth radiance errors in this paper) may cause the along- and cross-track biases in the SO_2 retrievals.

3.2 Solar irradiance errors

The solar irradiance measurements from a quartz volume diffuser depend on the viewing angle, the wavelength, as well as on the goniometry (incident azimuth and elevation angles of the Sun) onboard reflection diffuser (Veihelmann and Kleipool, 2006; Dobber et al., 2008). The viewing angle dependence, caused by calibration inaccuracies (Dobber et al., 2006), results in unequal responses for all viewing angles (up to 0.5 % error in UV2). The wavelength dependence in OMI UV2 spectral region has an amplitude of up to 0.1 % for the quartz volume diffuser (Dobber and Braak, 2010). The irradiance goniometry correction in the OMI GDPS software is realized by using the OPF calibration parameters derived from in-flight measurement data. However, when the azimuth angle on the diffuser falls below 18.3° or exceeds the value of 31.0°, large goniometry calibration inaccuracies may result from extrapolation errors (Dobber et al., 2008). In addition to these dependences, more noises can be introduced into the irradiance data because of increasing optical degradation (Dobber and Braak, 2010). These errors in solar irradiance are not constant and can cause the along-track stripes at specific viewing angles (one viewing angle corresponds to one cross-track position) (Veihelmann and Kleipool, 2006).

3.3 Earth radiance errors

The systematic errors in the Earth radiance can cause cross-track biases into retrieved SO_2 columns. The Earth radiance spectra, which are measured by the primary telescope mirror, mainly depend on viewing angle and optical degradation. The viewing angle dependence of the Earth radiance causes a

decrease of the value of level 1b radiance for the pixels at far off-nadir viewing angles (Dobber et al., 2008). This decrease has a subtle but significant effect on the OMI-retrieved SO_2 columns. Increasing optical degradation of the primary telescope mirror also introduces noises into the measured Earth radiance. This degradation is difficult to monitor and calibrate because no accurate standards over the full OMI wavelength range are readily available.

3.4 OMI row anomaly effects

Jaross and Warner have shown that no long-term degradation was observed in the earth radiance data during the three years after launch (from October 2004 to June 2007) (Jaross and Warner, 2008). However, the Earth radiance data at specific viewing angles have been severely affected by the row anomaly since June 2007 (Reference to the OMI row anomaly reports at http://www.knmi.nl/omi/research/product/rowanomaly-background.php). A row anomaly is an anomaly which affects the OMI measurements of Earth radiance at all wavelengths for particular viewing angles of OMI (one viewing angle corresponds to one cross-track position). The row anomaly affects the quality of OMI level 1b Earth radiance data and consequently the retrieved SO_2 columns.

The row anomaly have four different types of effects on OMI radiance spectra: (1) blockage effect that causes a decrease in the Earth radiance level for several viewing directions; (2) wavelength shift, which can be corrected by the OMI GDPS software version 1.1.3 (Voors, 2005); (3) Earth radiance from outside nominal field of view, which gives an additive error on the measured earth radiance; and (4) solar radiation that causes an increase in the Earth radiance level (http://www.knmi.nl/omi/research/product/rowanomaly-background.php). The OMI row anomaly is dynamic, varying irregularly with time and location (Dobber and Braak, 2010).

According to the row anomaly effects on Earth radiance, the row anomaly could be divided into two types: one is the row anomaly in the northern latitudes, and another is the row anomaly along the full orbit. The row anomaly in the northern latitudes, mainly caused by the reflection of sunlight into the nadir port, can increase the Earth radiance level. But the row anomaly along the full orbit, mainly caused by blocking object, can decrease (blockage effect) and increase (Earth radiance from outside nominal field of view) the Earth radiance level (result is a net decrease under most conditions). Note that when row anomaly along the full orbit occurs, the row anomaly in the northern latitudes comprises a decrease and increase in the Earth radiance signal (result is a net increase).

4 Correction approaches for improvement of SO_2 retrievals with row anomaly

The systematic measurement errors (Sects. 3.1.1 and 3.1.2), which vary with season and latitude, cause a background offset in the retrieved SO_2 column. In an effort to reduce these systematic measurement errors, Yang developed a residual correction approach before the final SO_2 column retrieval (Yang et al., 2007). This approach calculates a median residual from a sliding group of pixels of SO_2-free (smaller than 2 DU, DU = Dobson Units, 1 DU = 2.69×10^{16} molecules cm^{-2}) covering about 30° latitude along the orbit, and then subtracts the sliding median value for each spectral band and each cross-track position. With this approach, the retrieved SO_2 bias caused by the systematic errors can be reduced (Yang et al., 2007).

In addition to the systematic measurement errors, the SO_2 PBL column retrievals have been affected by the row anomaly since June 2007. The SO_2 biases caused by row anomaly cannot be effectively reduced by the residual correction approach developed by Yang (Yang et al., 2007). To improve global measurements of atmospheric SO_2 from OMI, we developed two effective correction approaches for improvement of SO_2 retrievals with row anomaly in the northern latitudes and along the full orbit, which are presented in this paper.

4.1 Row anomaly in the northern latitudes

Since May 2008, the cross-track positions 38–43 (1-based) have been affected by row anomaly in the northern latitudes, which results in an increase of the Earth radiance towards the northern end of the OMI orbit. To understand the characteristics of row anomaly in the northern latitudes, we took the residuals at wavelength pair P1 as a case study (cases of pairs P2 and P3 have similar row anomaly effects). Increase of the Earth radiance in the northern latitudes causes decrease in the measured N-pair value at pair P1 (Fig. 2), and subsequent decrease in the residuals (Fig. 3) and median residuals (Fig. 4) at P1. Because of the decrease of residuals in the northern latitudes, the residual correction approach with median residual from a sliding 30° latitude range is unsuitable when the row anomaly occurs.

The pixels from row 41 of orbit 23909, which were affected by the row anomaly in the northern latitudes, were used as a case study. In Fig. 4, point A is about 15° latitudes south of point C (inflection point), where the residual begins to decrease. As shown in Fig. 4, when the centered pixel in the sliding group of pixels covering 30° latitude approaching the point A, more pixels with low residual values are selected for median residual calculation. Those low residual values (subsequently low median residuals) between points A and C (Fig. 4) cause anomalous high values of corrected residuals from latitudes 5° N to 35° N (red line in black box in Fig. 4) and consequently anomalous high SO_2 columns (maximum

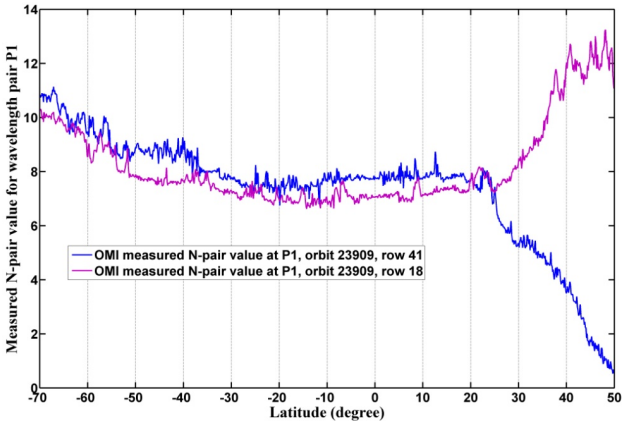

Fig. 2. The measured N-pair values at wavelength pair P1 affected (row 41 of orbit 23909, 12 January 2009) and not affected (row 18 of orbit 23909) by the row anomaly in the northern part of the OMI orbit.

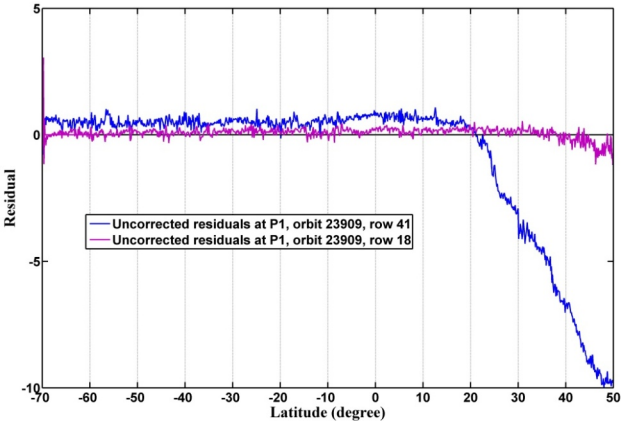

Fig. 3. The residuals at wavelength pair P1 affected (row 41 of orbit 23909, 12 January 2009) and not affected (row 18 of orbit 23909) by the row anomaly in the northern part of the OMI orbit. The black straight line represents the $Y = 0$ line.

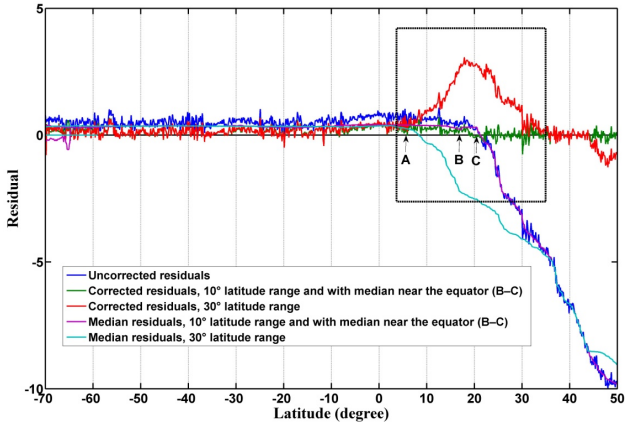

Fig. 4. The residuals (row 41, orbit 23909) at wavelength pair P1 processed with median residual from a sliding 30° latitude range and with those from a sliding 10° latitude range (for the pixels from points B to C, median residuals near the equator are used). Points A and B are respectively about 15° and 5° latitudes south of point C where the residual begins to be decreased because of row anomaly. The black straight line represents the $Y = 0$ line.

40 DU) (inside red ellipse in Fig. 6). In this case, high values of the SO_2 columns are not caused by strong SO_2 absorption, but rather by the underestimated median residuals from points A to C.

To make full use of the valid pixels not affected by the row anomaly from points A to C, median residuals from a smaller sliding window could better reduce the background errors. The question is what the suitable sliding window is. To answer this question, measurements from orbit 18637 (on 16 January 2008, little affected by the row anomaly) with latitudes ranging from $\sim 0°$ to $\sim +30°$ covering an oceanic area with low SO_2 emission were specifically selected. Median residuals from four different sliding window sizes covering 5°, 10°, 20° and 30° latitude range are calculated. Figure 5 shows that the median residuals from a sliding group of pixels (SO_2 column less than 2 DU) covering 20° and 10° latitude are consistent with those covering 30° latitude in the cross-track direction. It also demonstrates that the median residuals covering 5° latitude may not include sufficient information for background errors for residual correction. Therefore, the window with 10° latitude range was chosen for residual correction from points A to B of row 41 orbit 23909 (point B is about 5° latitude south of point C). It is worth noting that there is a trade-off between the window size and the effectiveness of the residual correction: too big a window for residual correction might result in poor correction under the row anomaly conditions, while too small a window might lead to reduction of the SO_2 information contained in the non-anomaly area.

For the pixels from points B to C (transition zone), a small window with less than 10° latitude range is needed. However, as shown in Fig. 5, such a window would not include the sufficient information for background errors for residual correction. In the extreme case of using the current line (SO_2 column less than 2 DU) as median residual calculation, the corrected residual will be equal to 0. Therefore, for the pixels from points B and C, we take the median residual near the Equator that is not affected by row anomaly as background values, like Krotkov who used the orbital equatorial averages for correction of SO_2 retrievals (Krotkov et al., 2006). For the pixels from point C to the terminator (latitude $> 85°$), we use the residual correction approach with median residual from a sliding 10° latitude range. Note that when the selected pixels approach the terminator, the window size for median residual is reduced to ensure approximately equal pixels on either side of the selected pixels along the orbit. After these procedures, the median residuals from points A

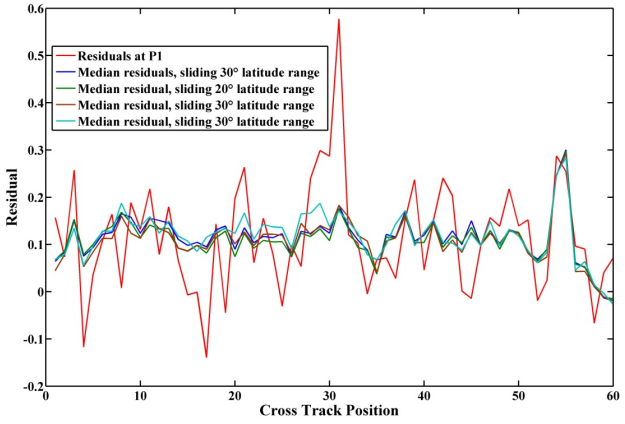

Fig. 5. Median residuals from four different sliding windows at wavelength pair P1 (swath line 1115, orbit 18637).

to C have no large decreases (Fig. 4), and the anomalous high SO_2 columns in the northern part of the orbit 23909 are removed (see Fig. 6). For the consistency of residual correction over the globe, residual correction with median residual from a sliding 10° latitude range is also applied to the OMI pixels in the southern latitudes.

The row anomaly in the northern latitudes varies with time and location, so the location of point C (inflection point) changes irregularly and needs to be determined for each affected row. The correction approach for wavelength pair P1 can also be applied to the residuals at wavelength pairs P2 and P3. The final SO_2 columns are the average of SO_2 columns of three wavelength pairs P1, P2, and P3. Note that due to the exacerbated UV-light penetration problem (Krotkov et al., 2006), coupled with row anomaly effects in the northern latitudes, the Earth radiances at latitudes higher than point C have little correlation with the SO_2 absorption and consequently SO_2 retrievals are in general not useful. It is also worth noting that some rows of the sample results in Fig. 6 are also slightly affected by the row anomaly along the full orbit, which will be discussed in Sect. 4.2.

4.2 Row anomaly along the full orbit

Since January 2009, SO_2 column retrievals have been severely affected by the row anomaly along the full orbit caused by blocking object (see Figs. 11 and 12). The anomaly results in decrease of OMI level 1b radiance in certain positions along the full orbit. Subsequently, the decreased radiance leads to large biases in the residuals (blue line in Fig. 10), which cannot be reduced by the correction approach described in Sect. 4.1.

Different from those affected by row anomaly in the northern latitudes, the measured N-pair values at P1 affected by the row anomaly along the full orbit are still positively correlated with the SO_2 columns. As shown in Fig. 9a, the measured N-pair values at P1 from row 39 of orbit 26166,

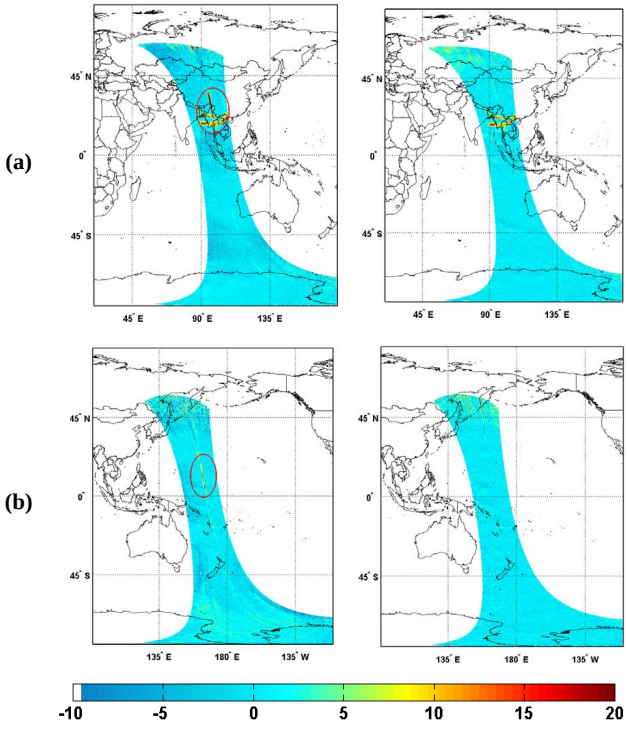

Fig. 6. SO_2 columns before (left panels) and after (right panels) correction for the case with row anomaly in the northern latitudes: **(a)** orbit 22965, 8 November 2008; **(b)** orbit 23909, 12 January 2009. Note that the missing data in the above maps are due to the value of SO_2 column being less than −10.

which are affected by the row anomaly along the full orbit, are consistent with those from row 18 not affected by the row anomaly. Both of them have a large increase in the northern $\sim 50°$ latitude because of the volcanic eruption (Sarychev volcano eruption starting on 11 June 2009, Global Volcanism Program). The reason for the good relationship between measured N-pair value and SO_2 column would be that the decrease of Earth radiance caused by row anomaly along the full orbit could be cancelled by using pair N values (N-pair $= N(\lambda_{\text{short}}) - N(\lambda_{\text{long}})$).

The residual biases along the full orbit are mainly caused by the anomalous O_3 column and underestimated LER, which are used as inputs to obtain the calculated N-pair value in the BRD algorithm. The OMTO3 O_3 column and LER are estimated by matching calculated radiances to the measured radiances at a pair of wavelengths (317.5 nm and 331.2 nm under most conditions). But the reduction of radiances caused by the row anomaly results in large biases in the retrieved O_3 column and LER (Fig. panels 7a and b). The biases existed in the O_3 columns as large as 30 % for orbit 26166 (increasing 1 % O_3 columns causes 5–15 % increase in retrieved SO_2 column), and the underestimate of LER is as large as 300 % (decreasing 1 % LER causes 0.2–1 % increase in retrieved SO_2 column). Because of the O_3 column errors

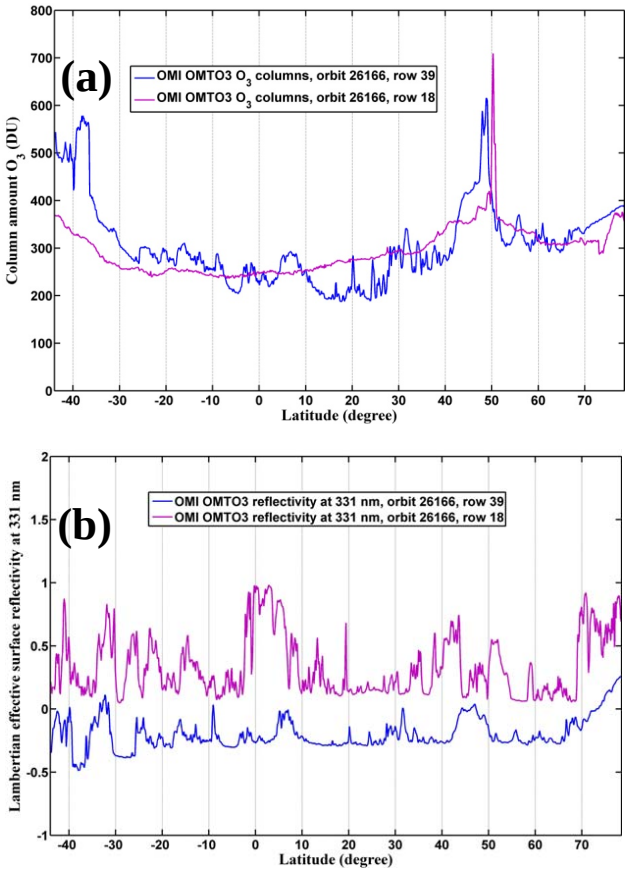

Fig. 7. OMI O_3 columns **(a)** and LER **(b)** from rows 39 and 18 of orbit 26166. Rows 39 and 18 are respectively affected and not affected by the row anomaly along the full orbit.

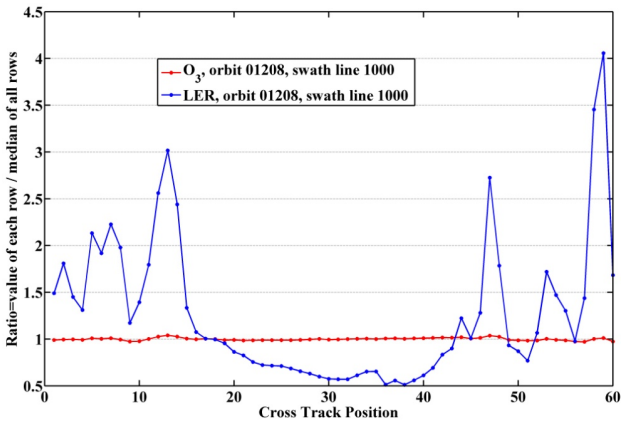

Fig. 8. Relative variation of O_3 column and LER with cross track position (6 October 2004, swath line 1000, orbit 01208, not affected by the row anomaly)

and underestimated LER (row 39, orbit 26166), the calculated N-pair values from TOMRAD model computation are inconsistent with those not affected by the row anomaly at row 18 (Fig. 9b). This inconsistency of calculated N-pair values causes large errors in the residuals at P1 (Fig. 10).

Consequently, reasonable O_3 columns are needed to obtain the calculated N-pair values for the rows affected by row anomaly over a full orbit. The atmospheric O_3, approximately 90 % of which resides in the stratosphere, changes little in nearby latitude in the same orbit (Fig. 8) (Smith, 1989). Therefore, the adjacent O_3 column not affected by the row anomaly could be chosen to represent the anomalous O_3 column at row 39 affected by the row anomaly. Then the calculated N-pair values are recalculated using adjacent O_3 columns as input. Consequently, large biases (caused by anomalous O_3 column) in the calculated N-pair values can be reduced, as shown in Fig. 9b.

In the case of using adjacent O_3 column to represent the anomalous O_3 column, the underestimate of LER causes a decrease in the calculated N-pair value compared with that using the adjacent O_3 column and LER (Fig. 9b). Different from the case of O_3 column retrieval, LER retrieved from 331 nm have large variation in nearby latitude because of different surface type and cloud cover, as shown in Fig. 8. Therefore, it is not suitable to use adjacent LER to represent the underestimated LER affected by the row anomaly. Fortunately, the decreases of the calculated N-pair values, which are caused by the underestimated LER, are almost unchanged along the full orbit compared with the calculated N-pair values using the adjacent O_3 column and LER (Fig. 9b). Therefore, the decreases in the calculated N-pair values could be removed by the residual correction approach with median residual from a sliding 10° latitude range. After processed with above mentioned procedures, the biases in the residuals at row 39 can be significantly reduced, as shown in Fig. 10. The corrected residuals at row 39 are consistent with those at row 18, which have a high value at $\sim 50°$ latitude north because of the volcanic eruption (Sarychev volcano eruption). Subsequently, the large biases in SO_2 columns of orbit 26166 can be effectively reduced by using the corrected residuals (see Fig. 11).

5 Results and discussion

5.1 Full orbit comparisons

As discussed in Sect. 4, the SO_2 biases caused by row anomaly can be effectively reduced after processed with our correction approaches. To evaluate the effectiveness of our correction approaches, several orbits covering different days with row anomaly effects from November 2008 to November 2009 were selected to compare the SO_2 columns before and after correction. As shown in Fig. 12, the SO_2 biases caused by row anomaly are reduced by modification of sliding median range and corrections of anomalous O_3 and LER effects.

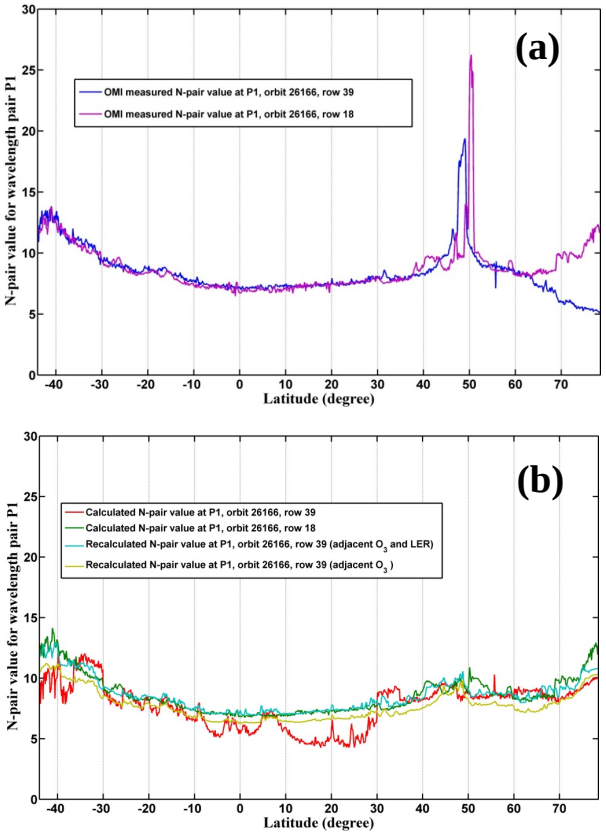

Fig. 9. (a) OMI measured N-pair values for rows 39 and 18 of orbit 26166; **(b)** calculated N-pair values for rows 39 and 18 of orbit 26166, and recalculated N-pair values for row 39 of orbit 26166. Rows 39 and 18 are respectively affected and not affected by the row anomaly along the full orbit.

To evaluate the effectiveness of our correction approaches for the case when low SO_2 columns are affected by the row anomaly, SO_2 columns of orbit 26166 (16 June 2009) with latitudes ranging from $\sim 0°$ to $\sim +20°$ (North Pacific Ocean area) were selected. With very low anthropogenic SO_2 emission and no volcanic eruption events (see Volcanic Activity Reports from Global Volcanism Program) in this area, the SO_2 columns should be near zero (Chin et al., 2000). Affected by the systematic measurement errors and row anomaly, the SO_2 columns are larger or less than 0 over the selected area. Under non-anomaly conditions, the biases in the SO_2 columns can be reduced by the median residuals from a sliding 30° latitude range. However, under the row anomaly conditions, this approach fails to reduce the row anomaly effects and the average SO_2 columns of orbit 26166 over the North Pacific Ocean area show significant increases at cross-track positions 31–41 and 48–50 (Fig. 13). But with our correction approaches for the row anomaly effects, these anomalous high SO_2 columns are reduced to near zero (Fig. 13), which demonstrates the effectiveness of our correction approaches for the case with low SO_2 columns affected by row anomaly.

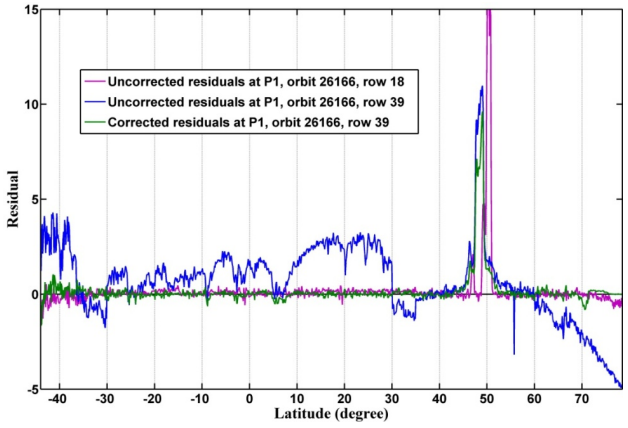

Fig. 10. The residuals from row 39 of orbit 26166 (16 June 2009) before and after correction for the row anomaly effects along the full orbit. Rows 39 and 18 are respectively affected and not affected by the row anomaly along the full orbit. The black straight line represents the $Y = 0$ line.

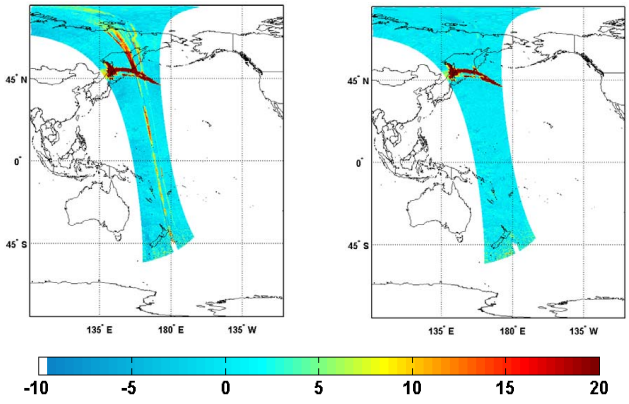

Fig. 11. SO_2 columns of orbit 26166 (16 June 2009) processed with median residual from a sliding 30° latitude range (left) and with the correction approaches for the row anomaly effects (right). Note that the missing data in the above maps are due to the value of SO_2 column being less than -10.

5.2 Limitations and discussion

5.2.1 Underestimation

When the row anomaly occurs, the residual correction approach with median residual from a sliding 10° latitude range is also applied to the pixels outside the row anomaly areas for the consistency of global residual correction presented in this paper. However, for the pixels not affected by row anomaly, there is a difference between SO_2 columns processed with median residual from a sliding 30° latitude range and with those from a sliding 10° latitude range. To evaluate the difference of sliding 30° and 10° latitude range on the retrieved SO_2 columns, the pixels from the northern area of orbit 18639 with latitudes ranging from $\sim 0°$ to $\sim +45°$ were

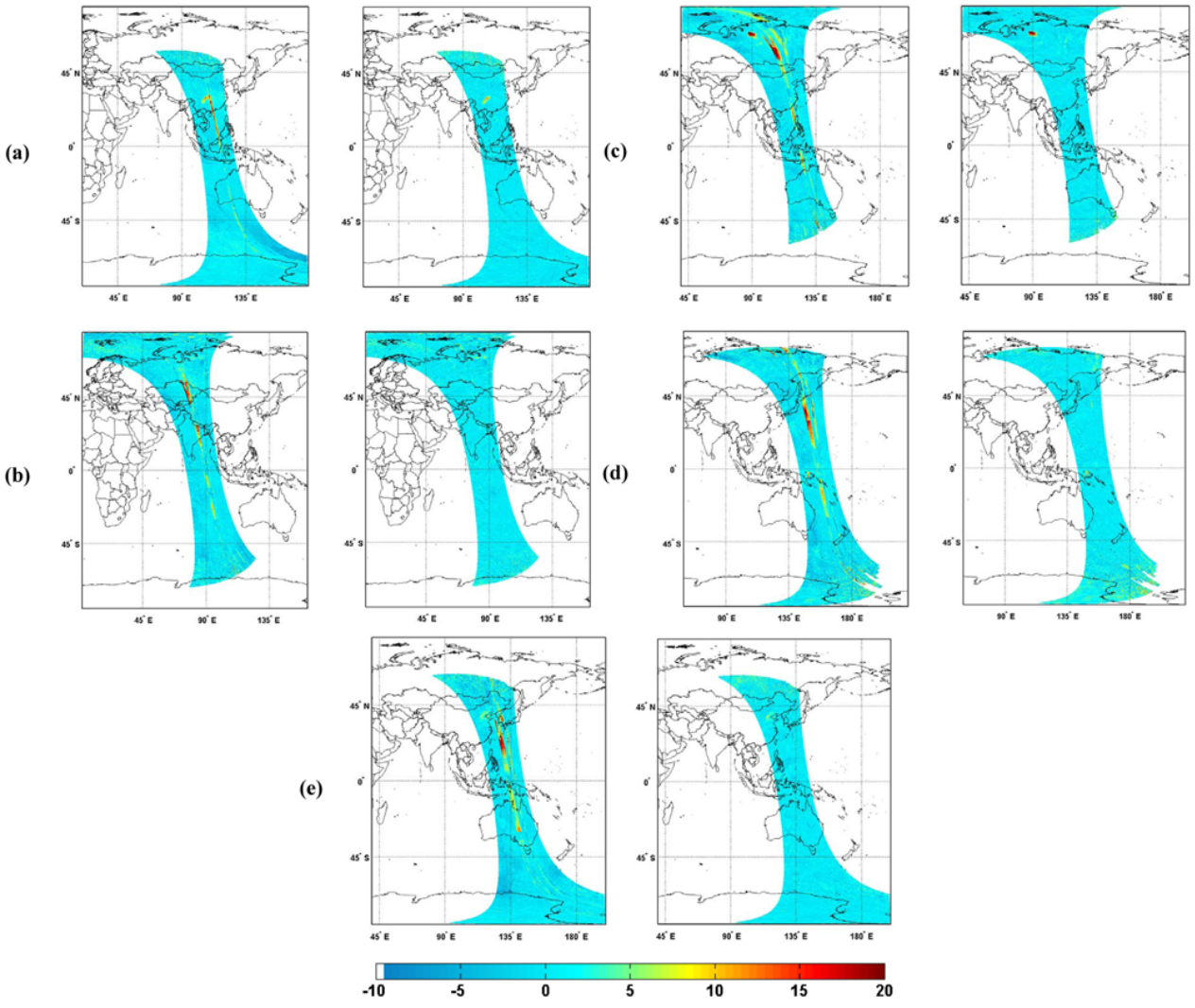

Fig. 12. Comparisons between SO_2 columns processed with median residual from a sliding 30° latitude range (left panels) and with the correction approaches for the row anomaly effects (right panels): **(a)** orbit 23911, 12 January 2009; **(b)** orbit 25179, 9 April 2009; **(c)** orbit 25731, 17 May 2009; **(d)** orbit 27783, 5 October 2009; **(e)** orbit 28279, 8 November 2009. Note that the missing data in the above maps are due to the value of SO_2 column being less than −10.

selected. For orbit 18639 (16 January 2008), the row anomalies have very little impact on the retrieved SO_2 columns, as eastern China has a large area of high SO_2 emissions (Fig. 14).

The SO_2 columns processed with median residual from a sliding 30° latitude range and with those from a 10° latitude range show good correlation for orbit 18639 (correlation coefficient reaching to 0.97) (Fig. 15). However, median residuals from a sliding 10° latitude range cause a slight underestimation for the case with high SO_2 column amounts. As shown in Fig. 15, in the case when the SO_2 columns are larger than 10 DU, the SO_2 columns processed with median residual from a sliding 10° latitude range are underestimated by 6 % to 16 % compared with those from a sliding 30° latitude range. The slope of regression line is larger than 1, which also proves the underestimation for orbit 18639. This underestimation is mainly related to a large area of high SO_2 emissions in eastern China. When the sliding range is changed from 30° latitude to 10° latitude in China, more pixels with high SO_2 columns are included for median residual calculation. Therefore, increased median residuals result in the slight underestimation of SO_2 column amount in China. For the case with low SO_2 columns (less than 10 DU), the underestimations are uncertain (overestimations may also occur) because of the uncertainty of median residuals from a sliding 30° and 10° latitude range.

We recognize that the precise SO_2 vertical column is important, and that the residual correction with median residual from a sliding 10° latitude range may actually affect the absolute value of the retrieved SO_2 column. However, actual

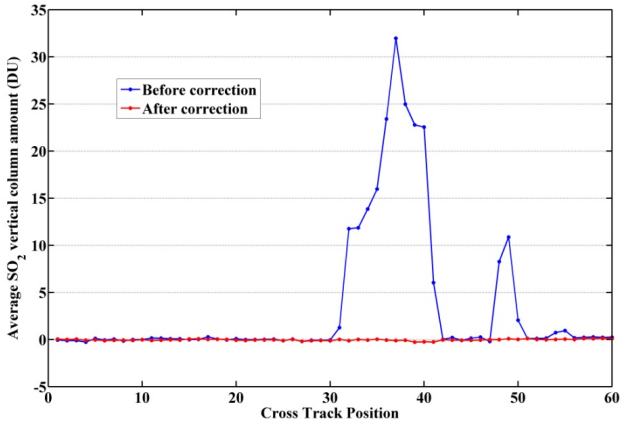

Fig. 13. Average SO_2 column amount for each row index before and after correction for the row anomaly effects. Data from orbit 26166 with latitudes ranging from $\sim 0°$ to $\sim +20°$ (North Pacific Ocean area).

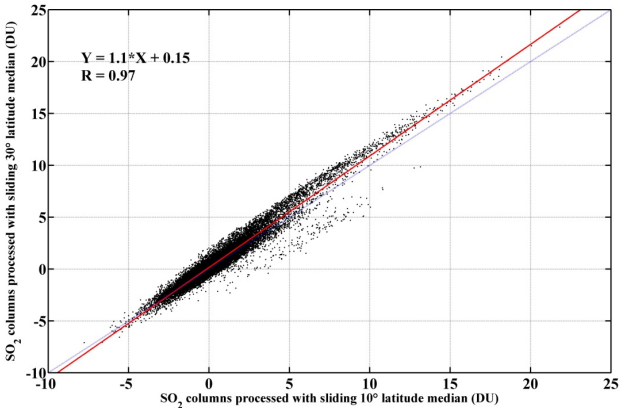

Fig. 15. Scatterplots of SO_2 columns processed with median residual from a sliding 30° latitude range versus with those from a sliding 10° latitude range for orbit 18639. The blue dashed line represents the $Y = X$ line. The red solid line denotes the regression line.

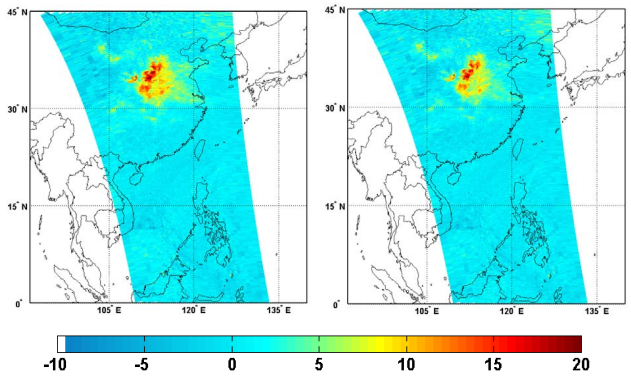

Fig. 14. SO_2 columns of orbit 18639 (16 January 2008) with latitudes ranging from $\sim 0°$ to $\sim +45°$. (Left) results processed with median residual from a sliding 30° latitude range, (right) results processed with median residual from a sliding 10° latitude range.

background errors in the residuals are dynamic and difficult to obtain over the globe. Various mathematical approaches for background errors correction may have different effects on the accurate retrieval of SO_2 column. Current SO_2 retrieval approaches (BRD, LF and DOAS) can only obtain the relative SO_2 columns, but not absolute SO_2 results. Therefore, the residual correction approach with median residual from a sliding 10° latitude range can be considered as an effective approach for the case when the row anomaly occurs. For the orbits that were not affected by the row anomaly (before June 2007), we recommend using the residual correction approach developed by Yang (Yang et al., 2007), which calculates median residual from a sliding 30° latitude range.

5.2.2 O_3 column and LER errors

In the BRD algorithm, O_3 column and LER used as inputs can interfere with SO_2 retrieval in the ultraviolet band. Under non-anomaly conditions, the interference from O_3 absorption causes negative SO_2 column. Under the row anomaly conditions, the decrease and increase of OMI measured radiances since June 2007 result in large biases in the retrieved O_3 column and LER, and subsequently make it more difficult to get accurate SO_2 retrieval.

The row anomaly effects on measured radiances lead to the anomalous O_3 column and underestimated LER at 331 nm. In this paper, we utilize the adjacent O_3 column not affected by the row anomaly to reduce the SO_2 biases caused by the anomalous O_3 column, and use residual correction with median residual from a sliding 10° latitude range to reduce the SO_2 biases caused by the underestimated LER. However, in the special case when there is a large difference between the adjacent O_3 column and the actual O_3 columns in anomaly area, the adjacent O_3 column can lead to large bias in the retrieved SO_2 column. Besides, if the row anomaly causes a very large reduction in the measured radiance, the remaining LER error after residual correction can still lead to large bias in the retrieved SO_2 column.

When the measured radiance data are affected by very severe row anomaly, the SO_2 columns after our correction approaches will still have large biases. In the extreme case, the row anomaly effects are so large that the measurement N-pair values have no correlation with the SO_2 columns. In this case, new effective corrections for the affected Earth radiance at specific viewing angles are needed.

6 Conclusions

We have presented two correction approaches for improvement of OMI SO_2 PBL retrieval with row anomaly in the northern latitudes and along the full orbit. The sample results have demonstrated the success of our correction approaches, with which large biases in the retrieved SO_2 columns from

BRD algorithm are greatly reduced so that consistent SO_2 values are achieved both inside and outside of row anomaly areas. The correction approaches for the row anomaly effects can extend the valid range of OMI SO_2 PBL data produced using the BRD algorithm.

In addition to the instrument measurement errors, the retrieval algorithm model errors, which are not discussed in this study, can bring about more complex biases in retrieved SO_2 columns. Over the years, a number of algorithms (DOAS, BRD, LF, etc.) for determining SO_2 from satellite instruments have been developed in the ultraviolet spectral region (310 nm to 340 nm). However, the retrieved SO_2 columns using these algorithms are affected by the nonlinear effect (Yang et al., 2007), because they assume an approximate linear relationship between SO_2 columns and the reflected TOA radiation. This linear approximation leads to an underestimation of the actual SO_2 column by the BRD, DOAS and LF algorithms, especially with a large SO_2 column. Besides, O_3, which is a strong absorber in the ultraviolet spectral region, needs to be distinguished from SO_2, which is small in the atmosphere under most conditions and has little absorption effect on the ultraviolet radiance. Therefore, the quantitative retrieval of SO_2 column, especially low near-surface SO_2 column, needs further study.

Acknowledgements. This research was supported by the Strategic Pilot Project of Chinese Academy of Sciences (B) (Grant No: XDB05030100). The authors would like to thank two anonymous reviewers for their assistance in evaluating this paper. We are grateful to the members of the OMI science team for providing OMI level 1b Earth radiance and solar irradiance data, as well as OMI level 2 O_3 and SO_2 products (http://disc.gsfc.nasa.gov/). Thanks also to Remco Braak for communications of OMI data errors through emails.

Edited by: D. Loyola

References

Bhartia, P. K. and Wellemeyer, C. W.: TOMS-V8 total ozone algorithm, in: OMI Algorithm Theoretical Basis Document, OMI Ozone Products, edited by: Bhartia, P. K., Greenbelt, MD: NASA/Goddard Space Flight Center, 2002.

Bogumil, K., Orphal, J., Homann, T., Voigt, S., Spietz, P., Fleischmann, O. C., Vogel, A., Hartmann, M., Kromminga, H., Bovensmann, H., Frerick, J., and Burrows, J. P.: Measurements of molecular absorption spectra with the SCIAMACHY preflight model: instrument characterization and reference data for atmospheric remote-sensing in the 230–2380 nm region, J. Photoch. Photobio. A, 157, 167–184, doi:10.1016/S1010-6030(03)00062-5, 2003.

Carn, S. A., Krueger, A. J., Krotkov, N. A., Yang, K., and Levelt, P. F.: Sulfur dioxide emissions from Peruvian copper smelters detected by the Ozone Monitoring Instrument, Geophys. Res. Lett., 34, L09801, doi:10.1029/2006GL029020, 2007.

Chin, M., Savoie, D. L., Huebert, B. J., Bandy, A. R., Thornton, D. C., Bates, T. S., Quinn, P. K., Saltzman, E. S., and De Bruyn, W. J.: Atmospheric sulfur cycle simulated in the global model GOCART: Comparison with field observations and regional budgets, J. Geophys. Res., 105, 24689–24712, doi:10.1029/2000JD900385, 2000.

Corradini, S., Merucci, L., and Prata, A. J.: Retrieval of SO_2 from thermal infrared satellite measurements: correction procedures for the effects of volcanic ash, Atmos. Meas. Tech., 2, 177–191, doi:10.5194/amt-2-177-2009, 2009.

Cullis, C. F. and Hirschler, M. M.: Atmospheric Sulfur- Natural and Man-made sources, Atmos. Environ., 14, 1263–1278, 1980.

Dave, J. V.: Meaning of successive iteration of the auxiliary equation of radiative tranfer, Astrophys. J., 140, 1292–1303, 1964.

Dobber, M. R. and Braak, R.: Known instrumental effects that affect the OML1B product of the Ozone Monitoring Instrument on EOS Aura, last update: 17 December 2010.

Dobber, M. R., Dirksen, R. J., Levelt, P. F., Van den Oord, G. H. J., Voors, R. H. M., Kleipool, Q., Jaross, G., Kowalewski, M., Hilsenrath, E., Leppelmeier, G. W., de Vries, J., Dierssen, W., and Rozemeijer, N. C.: Ozone Monitoring Instrument Calibration, IEEE T. Geosci. Remote, 44, 1209–1238, doi:10.1109/TGRS.2006.869987, 2006.

Dobber, M. R., Kleipool, Q., Dirksen, R. J., Levelt, P. F., Jaross, G., Taylor, S. L., Kelly, T. J., Flynn, L. E., Leppelmeier, G. W., and Rozemeijer, N. C.: Validation of ozone monitoring instrument level 1b data products, J. Geophys. Res., 113, D15S06, doi:10.1029/2007JD008665, 2008.

Finlayson-Pitts, B. J. and Pitts, J. N.: Chemistry of the Upper and Lower Atmosphere, Academic Press, San Diego, USA, 2000.

IPCC: Climate Change 2001: The Scientific Basis, Contribution of Working Group I to the Third Assessment Report of the Intergovernmental Panel on Climate Change (IPCC), edited by: Houghton, J. T., Ding, Y., Griggs, D. J., Noguer, M., van der Linden, P. J., Dai, X., Maskell, K., and Johnson, C. A., Cambridge University Press, Cambridge, UK and New York, NY, USA, 881 pp., 2001.

Jaross, G. and Warner, J.: Use of Antarctica for validating reflected solar radiation measured by satellite sensors, J. Geophys. Res., 113, D16S34, doi:10.1029/2007JD008835, 2008.

Khokhar, M. F., Frankenberg, C., Van Roozendael, M., Beirle, S., Kühl, S., Richter, A., Platt, U., and Wagner, T.: Satellite observations of atmospheric SO_2 from volcanic eruptions during the time-period of 1996–2002, Adv. Space Res., 36, 879–887, doi:10.1016/j.asr.2005.04.114, 2005.

Krotkov, N. A., Carn, S. A., Krueger, A. J., Bhartia, P. K., and Yang, K.: Band Residual Difference Algorithm for Retrieval of SO_2 From the Aura Ozone Monitoring Instrument (OMI), IEEE T. Geosci. Remote, 44, 1259–1266, 2006.

Krotkov, N. A., McClure, B., Dickerson, R. R., Carn, S. A., Li, C., Bhartia, P. K., Yang, K., Krueger, A. J., Li, Z. Q., Levelt, P. F., Chen, H. B., Wang, P. C., and Lu, D.: Validation of SO_2 retrievals from the Ozone Monitoring Instrument over NE China, J. Geophys. Res., 113, D16S40, doi:10.1029/2007JD008818, 2008.

Krueger, A. J.: Sighting of El Chichón Sulfur Dioxide Clouds with the Nimbus 7 Total Ozone Mapping Spectrometer, Science, 220, 1377–1379, 1983.

Krueger, A. J., Krotkov, N. A., Datta, S., Flittner, D., and Dubovik, O.: SO_2, in: OMI Algorithm Theoretical Basis Document, OMI

Trace Gas Algorithms, 2, edited by: Chance, K., Smithsonian Astrophysical Observatory, Cambridge, MA, 49–59, 2002.

Lee, C., Richter, A., Weber, M., and Burrows, J. P.: SO_2 Retrieval from SCIAMACHY using the Weighting Function DOAS (WF-DOAS) technique: comparison with Standard DOAS retrieval, Atmos. Chem. Phys., 8, 6137–6145, doi:10.5194/acp-8-6137-2008, 2008.

Levelt, P. F., Van der Oord, G. H. J., Dobber, M. R., Malkki, A., Visser, H., de Vries, J., Stammes, P., Lundell, J. O. V., and Saari, H.: The Ozone Monitoring Instrument, IEEE T. Geosci. Remote, 44, 1093–1101, 2006.

Li, C., Zhang, Q., Krotkov, N. A., Streets, D. G., He, K. B., Tsay, S. C., and Gleason, J. F.: Recent large reduction in sulfur dioxide emissions from Chinese power plants observed by the Ozone Monitoring Instrument, Geophys. Res. Lett., 37, L08807, doi:10.1029/2010GL042594, 2010.

McPeters, R. D., Labow, G. J., and Logan, J. A.: Ozone climatological profiles for satellite retrieval algorithms, J. Geophys. Res., 112, D05308, doi:10.1029/2005JD006823, 2007.

Platt, U.: Differential optical absorption spectroscopy (DOAS), in: Air Monitoring by Spectroscopic Techniques, Chemical Analysis Series, edited by: Sigrist, M. W., John Wiley & Sons, Inc., 127, 27–84, 1994.

Platt, U. and Stutz, J.: Differential Optical Absorption Spectroscopy: Principles and Applications, Physics of Earth and Space Environments, Hardcover, Springer, Verlag Berlin Heidelberg, 593 pp., 2008.

Realmuto, V. J., Abrams, M. J., Buongiorno, M. F., and Pieri, D. C.: The use of multispectral thermal infrared image data to estimate the sulfur dioxide flux from volcanoes: A case study from Mount Etna, Sicily, 29 July 1986, J. Geophys. Res., 99, 481–488, doi:10.1029/93JB02062, 1994.

Richter, A., Wittrock, F., and Burrows, J. P.: SO_2 measurements with SCIAMACHY, Atmospheric Science Conference, Eur.Space Agency Cent. for Earth Obs., Frascati, Italy, 8–12 May 2006.

Rix, M., Valks, P., Van Gent, J., Van Roozendael, M., Spurr, R., Hao, N., Emmadi, S., and Zimmer, W.: Monitoring of volcanic SO_2 emissions using the GOME-2 satellite instrument, Geophys. Res. Abstr., EGU2010-4754, EGU General Assembly 2010, Vienna, Austria, 2010.

Seinfeld, J. H. and Pandis, S.: Atmospheric Chemistry and Physics, John Wiley & Sons, New York, USA, 1998.

Smith, R. C.: Ozone, Middle Ultraviolet-Radiation and the Aquatic Environment, Photochem. Photobiol., 50, 459–468, 1989.

Van den Oord, G. H. J., Voors, R. H. M., and De Vries, J.: The Level 0 to Level 1B processor for OMI radiance, irradiance and calibration data, in: OMI Algorithm Theoretical Basis Document, OMI instrument, Level 0–1b processor, Calibration & Operations, edited by: Levelt, P. F., 2002.

Van den Oord, G. H. J., Rozemeijer, N. C., Schenkelaars, V., Levelt, P. F., Dobber, M. R., Voors, R. H. M., Claas, J., De Vries, J., Ter Linden, M., De Haan, C., and de Berg, T. V.: OMI level 0 to 1b processing and operational aspects, IEEE T. Geosci. Remote, 44, 1380–1397, doi:10.1109/TGRS.2006.872935, 2006.

Veihelmann, B. and Kleipool, Q.: Reducing Along-Track Stripes in OMI-Level 2 Products, TN-OMIE-KNMI-785, 24 pp., 2006.

Voors, R.: OMI GDPS Algorithm to correct for wavelength shifts due to inhomogeneous slit illumination, TN-OMIE-KNMI-680, Issue 1, 2005.

Wellemeyer, C. G., Taylor, S. L., Seftor, C. J., McPeters, R. D., and Bhartia, P. K.: A correction for total ozone mapping spectrometer profile shape errors at high latitude, J. Geophys. Res., 102, 9029–9038, 1997.

Yan, H. H., Chen, L. F., Tao, J. H., Han, D., Su, L., and Yu, C.: SO_2 long-term monitoring by satellite in the Pearl River Delta, Journal of Remote Sensing, 16, 390–404, 2012.

Yang, K., Krotkov, N. A., Krueger, A. J., Carn, S. A., Bhartia, P. K., and Levelt, P. F.: Retrieval of large volcanic SO_2 columns from the Aura Ozone Monitoring Instrument: comparison and limitations, J. Geophys. Res., 112, D24S43, doi:10.1029/2007JD008825, 2007.